5 Vectorial Pulse Width Modulation for Basic Three-Phase Inverters

Previous chapters have explained the need for pulse width modulation (PWM) control of three-phase converters and presented some conventional methods that generate PWM on each phase independently. Some limitations in its practical implementation have stimulated efforts to find other principles to generate PWM controls. The most remarkable is the analysis of the three-phase inverter in the complex plane by the Vector Space theory. Understanding the mathematical representation of the inverter operation in the complex plane provided a tool for the generation of a new PWM algorithm called *Space Vector Modulation* (SVM). (Note the difference between a vector space, which means a space of vectors, and a space vector, which means a vector with a spatial displacement.)

SVM has become a standard for medium- and high-power switching converters in both industry and university. The last 20 years have provided a large volume of publications that fully define SVM theory. Implementation on different digital platforms has been considered and some dedicated integrated circuits have already been developed on the basis of this principle. The SVM theory initially developed for three-phase voltage-source inverters has been extended with new applications to other three-phase topologies. Such methods will be presented in later chapters.

5.1 REVIEW OF SPACE VECTOR THEORY

5.1.1 HISTORY AND EVOLUTION OF THE CONCEPT

The first vectorial representation of three-phase systems was introduced by Park [1], Kron [2], and Stanley [3]. They showed the separation of effects on two axes at the operation of a three-phase electrical drive. First, Park [1] replaced the variables associated to the stator windings with variables of fictitious windings rotating with the rotor. This work can be considered the base for the well-known theory of vector control or field-orientation control for induction and synchronous drives. In the late 1930s, Stanley [2] used the same idea for induction machine drives but he replaced the rotor variables to a frame fixed on the stator. During the 1960s, the advent of thyristors led to the systematic use of the Space Vector theory to analyze and control three-phase electrical drives. Kovacs and Racz [4] provided mathematical treatment along with a physical description and understanding of

machine drive transients even in the cases in which machines were fed through electronic converters.

Space Vector-derived methods were widely used by the industry in the early 1970s and numerous books have presented this theory. Stepina [5] and Serrano-Iribarnegaray [6] suggested the use of the *Space Phasor* to analyze electrical machines. The Space Phasor concept is now used mainly for current and flux measures when analyzing electrical machines.

It was again the semiconductor technology that pushed for more consideration of the vectorial analysis theory in the early 1980s. Development and intensive use of the first microprocessors in industry opened new research areas to find the most appropriate implementation algorithms for conventional issues of PWM generation, current control, or field-orientation-based control of electrical drives. Murai and Tsunehiro [7] reported in 1983 an improved PWM method derived from vectorial analysis of the operation of a three-phase inverter. A few years later, different researchers [8–11], considering all three phases in a unique vector, developed the SVM theory further to control the inverter in open loop and, later, in closed loop. The new method provided great advantages in digital implementation with the newly arrived microcontrollers.

5.1.2 THEORY: VECTORIAL TRANSFORMS AND ADVANTAGES

A three-phase system defined by $u_x(t)$, $u_y(t)$, and $u_z(t)$ can be represented uniquely by a rotating vector u_S in the complex plane.

$$u_s = \frac{2}{3}[u_x(t) + au_y(t) + a^2u_z(t)] \tag{5.1}$$

where $a = e^{j(2\pi/3)}$ and $a^2 = e^{j(4\pi/3)}$.

All vectors in the complex plane form a space of vectors [12]. The mathematical theory of vector spaces is next employed to provide an instrument for analysis.

A *base* within a vector space consists of a system of vectors B (b_1,b_2,b_3) that is a unique representation of any member V of that vector space as a linear combination of vectors from B. For instance,

$$\vec{V} = b_1(\omega_j)v_d + b_2(\omega_j)v_q + b_3(\omega_j)v_0 \tag{5.2}$$

or

$$\vec{V} = b_1(\omega_j)v_d + b_2(\omega_j)v_q \tag{5.3}$$

where v_d, v_q, and v_0 are also called co-ordinates. If the vector space has a finite dimension, then all possible bases have the same number of elements. The dimension of a vector space refers to the number of vectors within any base. When applied to three-phase power systems or power converters, the dimension of the vector space is three, which means that any base has three elements. A base is

orthonormalized if all its vectors are unitary and any two different vectors are orthogonal. The mathematical theory of vector spaces also provides tools for making transformations between different bases of the same vector space. These transformations are unique and reversible and can have linear or rotational effects on the vectors.

All the previously reported papers in the three-phase power electronics indirectly consider the orthogonal base vectors as

$$[b_1(\omega_i)]^T = \frac{3}{2}\left[\cos \omega_i t \quad \cos\left[\omega_i t - \frac{2\pi}{3}\right] \quad \cos\left[\omega_i t - \frac{4\pi}{3}\right] \right] \tag{5.4}$$

$$[b_2(\omega_i)]^T = \frac{3}{2}\left[\sin \omega_i t \quad \sin\left[\omega_i t - \frac{2\pi}{3}\right] \quad \sin\left[\omega_i t - \frac{4\pi}{3}\right] \right] \tag{5.5}$$

$$[b_3(\omega_i)]^T = \frac{3}{2}[1 \quad 1 \quad 1] \tag{5.6}$$

The selection of this set of vectors is not unique. Coefficients and functions within each term may have other forms depending on where they are to be aplied. In our case, in a three-phase system, we would like to take advantage of sin and cos functions because we know that our phase voltages have this type of variation and we hope to separate DC quantities (constant numbers) as coordinates of Equation (5.2). The discontinuous PWM algorithms presented in Chapter 3 can enlarge the field of application of this theory. The ON-time variation is represented by the discontinuous function, depending on the phase coordinates and the conventional outputs of the vector control algorithm. Selecting base vectors characterized by that type of variation would provide a mathematical instrument for directly transforming the quasi-DC quantities of the vector control algorithm into an ON-time variation function that can be used to control the PWM generator.

Another example can refer to the selection of the coefficients in [2]. Engineers analyzing power systems take advantage of this property by defining base vectors and transform coefficients from either *power conservation* or *magnitude conservation* constraints. Thus, the coefficient $(3/2)$ from Equation (5.4) and Equation (5.5) is calculated to preserve the magnitude of the vector in the complex plane, but some engineers use a coefficient of *sqrt*$(3/2)$ to preserve power through the transform.

Basically, this theory says that we can decompose any vector in the complex plane in a form shown by Equation (5.2) where the base vectors may have a form as in Equation (5.4), Equation (5.5), and Equation (5.6). The coordinate v_d of Equation (5.2) is the result of that part of the first phase voltage that follows $\cos \omega_i t$ added to that part of the second phase that follows $\cos(\omega_i t - 2\pi/3)$ and to that part of the third phase that follows $\cos(\omega_i t - 4\pi/3)$.

Similarly, the coordinate v_q of Equation (5.2) is the result of that part of the first phase voltage that follows $\sin \omega_i t$ added to that part of the second phase that follows $\sin(\omega_i t - 2\pi/3)$ and to that part of the third phase that follows $\sin(\omega_i t - 4\pi/3)$. Finally, the quasi-DC components in all the phases are added in v_0. Replacing

Equation (5.4), Equation (5.5), and Equation (5.6) in Equation (5.2) yields a relationship between coordinates in different bases:

$$
\vec{V} = \begin{bmatrix} u_x \\ u_y \\ u_z \end{bmatrix} = \frac{3}{2} \begin{bmatrix} \cos \omega_i t \\ \cos\left(\omega_i t - \dfrac{2\pi}{3}\right) \\ \cos\left(\omega_i t - \dfrac{4\pi}{3}\right) \end{bmatrix} v_d + \frac{3}{2} \begin{bmatrix} \sin \omega_i t \\ \sin\left(\omega_i t - \dfrac{2\pi}{3}\right) \\ \sin\left(\omega_i t - \dfrac{4\pi}{3}\right) \end{bmatrix} v_q + \frac{1}{2} \begin{bmatrix} 1 \\ 1 \\ 1 \end{bmatrix} v_0
$$

$$
\Longrightarrow \begin{bmatrix} u_x \\ u_y \\ u_z \end{bmatrix} = \frac{3}{2} \begin{bmatrix} \cos \omega_i t & \sin \omega_i t & \dfrac{1}{3} \\ \cos\left(\omega_i t - \dfrac{2\pi}{3}\right) & \sin\left(\omega_i t - \dfrac{2\pi}{3}\right) & \dfrac{1}{3} \\ \cos\left(\omega_i t - \dfrac{4\pi}{3}\right) & \sin\left(\omega_i t - \dfrac{4\pi}{3}\right) & \dfrac{1}{3} \end{bmatrix} \begin{bmatrix} v_d \\ v_q \\ v_0 \end{bmatrix}
$$

$$\tag{5.7}$$

This is the core idea of a vector transformation from coordinates $u_x(t)$, $u_y(t)$, $u_z(t)$ to coordinates $u_d(t)$, $u_q(t)$, $u_0(t)$ or vice versa. This operation of transforming a three-phase system in a unique vector followed by the transformation of the orthogonal vector coordinates in quasi-DC coordinates $(d, q, 0)$ is known as *Park/Clarke transforms* for three-phase systems.

5.1.2.1 Clarke Transform

First, let us transform the phase measures into orthogonal coordinates with a third homopolar (or zero sequence) coordinate. Any vector in the complex plane can be decomposed into two orthogonal coordinates (U_α, U_β) and a homopolar coordinate U_0.

$$
\begin{bmatrix} U_\alpha \\ U_\beta \\ U_0 \end{bmatrix} = \frac{2}{3} \begin{bmatrix} 1 & -\dfrac{1}{2} & -\dfrac{1}{2} \\ 0 & \dfrac{\sqrt{3}}{2} & -\dfrac{\sqrt{3}}{2} \\ \dfrac{1}{2} & \dfrac{1}{2} & \dfrac{1}{2} \end{bmatrix} \begin{bmatrix} u_x \\ u_y \\ u_z \end{bmatrix}
\tag{5.8}
$$

where (U_α, U_β) form an orthogonal two-phase system and $u_s = U_\alpha + jU_\beta$. If the system of phase voltages is symmetrical, the homopolar term equals zero and it can miss within the previous transform. Moreover, this transform is unique, as shown in Figure.5.1.
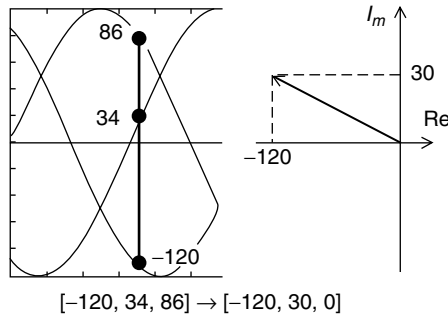
FIGURE 5.1 Derivation of a vector equivalent to a three-phase system.

5.1.2.2 Park Transform

This transform is not directly necessary for the presentation of the SVM algorithm, but is often used by electrical engineers in vector control of power converters. The two coordinates (α, β) are transformed through a vector rotation, with the rotational frequency identical to the electrical frequency.

$$
\begin{bmatrix} U_d \\ U_q \\ U_0 \end{bmatrix} = \begin{bmatrix} \cos\theta & \sin\theta & 0 \\ -\sin\theta & \cos\theta & 0 \\ 0 & 0 & 1 \end{bmatrix} \begin{bmatrix} U_\alpha \\ U_\beta \\ U_0 \end{bmatrix}
\tag{5.9}
$$

Frequently, these two transforms are used in a single transform stage that coincides with the vector space theory introduced in the beginning (5.7)

$$
\begin{bmatrix} U_d \\ U_q \\ U_0 \end{bmatrix} = \frac{2}{3} \begin{bmatrix} \cos\theta & \cos\left[\theta - \dfrac{2\pi}{3}\right] & \cos\left[\theta - \dfrac{4\pi}{3}\right] \\ \sin\theta & \sin\left[\theta - \dfrac{2\pi}{3}\right] & \sin\left[\theta - \dfrac{4\pi}{3}\right] \\ \dfrac{1}{2} & \dfrac{1}{2} & \dfrac{1}{2} \end{bmatrix} \begin{bmatrix} u_x \\ u_y \\ u_z \end{bmatrix}
\tag{5.10}
$$

Each of these transforms has an inverse that allows transformation from the orthogonal coordinates to the phase measures. The general inverse transform is given by

$$
\begin{cases} u_x(t) = \mathrm{Re}[u_s] + u_0(t) \\ u_y(t) = \mathrm{Re}[a^2 u_s] + u_0(t) \\ u_z(t) = \mathrm{Re}[a\, u_s] + u_0(t) \end{cases}
\tag{5.11}
$$

where $u_0(t) = \frac{1}{3}[u_x(t) + u_y(t) + u_z(t)]$ represents the homopolar component. Particular forms are also available for Park and Clarke inverse transforms.

5.1.3 APPLICATION TO THREE-PHASE CONTROL SYSTEMS

This mathematical representation of three-phase measures treats the analysis of the three-phase system as a whole, instead of considering equations for each phase individually. Many control methods for three-phase systems have been derived from this mathematical approach.

Electrical drives (induction machine or synchronous machine drives) are controlled by the so-called field-orientation principle (Figure 5.2a). The three-phase
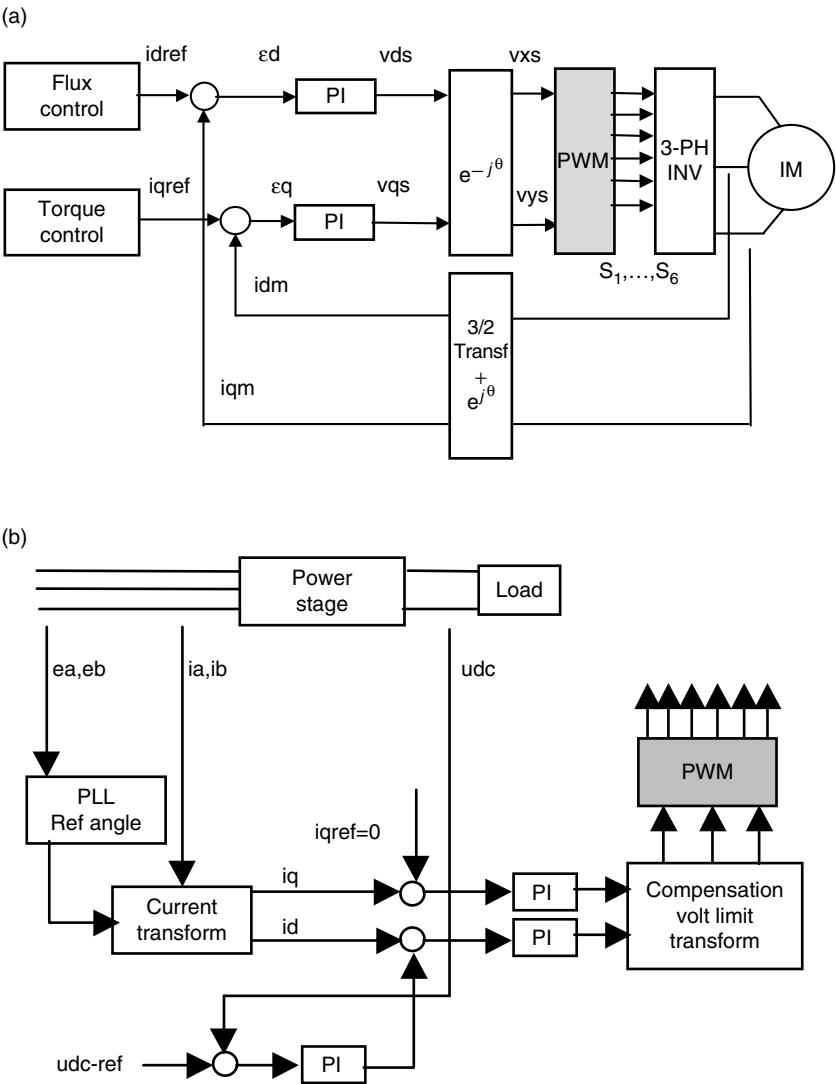
(a)

(b)

FIGURE 5.2 Examples of application of vectorial representation in control (a) motor drive controller; (b) grid interactive controller.

grid interfaces or AC/DC converters (Figure 5.2b) are nowadays seen as active filtering systems controlled by the instantaneous power components ($p-q$) theory. All these systems use PWM algorithms in the final control stage.

5.2 VECTORIAL ANALYSIS OF THE THREE-PHASE INVERTER

5.2.1 MATHEMATICAL DERIVATION OF THE CURRENT SPACE VECTOR TRAJECTORY IN THE COMPLEX PLANE FOR SIX-STEP OPERATION (WITH *RESISTIVE* AND *RESISTIVE-INDUCTIVE* LOADS)

The three-phase inverter presented in Figure 5.3 is built of six insulated gate bipolar transistors (IGBTs), but it can be made with any other power-switching device, depending on the voltage and current ratings.

Figure 5.4 presents the appropriate output voltages without PWM. This is the so-called *six-step operation* and it is also the simplest and oldest control method for this type of power converter. Different switching states are given in the figure with a digital code (for example: 1 0 1), showing whether the high-side IGBT is ON (for 1) or the low-side device is ON (for 0). Another possible notation uses a sign to show where the pole terminals (A, B, C) are connected.

Each state of the power converter leads to a switching vector in the complex plane. There are thus six active switching vectors $V_1,\ldots,V_6$ equally sharing six sectors within the complex plane (Figure 5.5).

The vectorial analysis of the operation of this system is first developed for an inductive three-phase load. Each phase current waveform can be derived by the integral of each phase voltage equation.

$$\begin{cases} v_\text{a} = L_s \dfrac{\mathrm{d}i_\text{a}}{\mathrm{d}t} \\ v_\text{b} = L_\text{s} \dfrac{\mathrm{d}i_\text{b}}{\mathrm{d}t} \\ v_\text{c} = L_\text{s} \dfrac{\mathrm{d}i_\text{c}}{\mathrm{d}t} \end{cases} \tag{5.12}$$
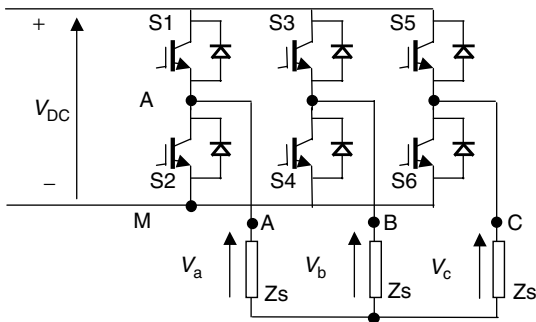

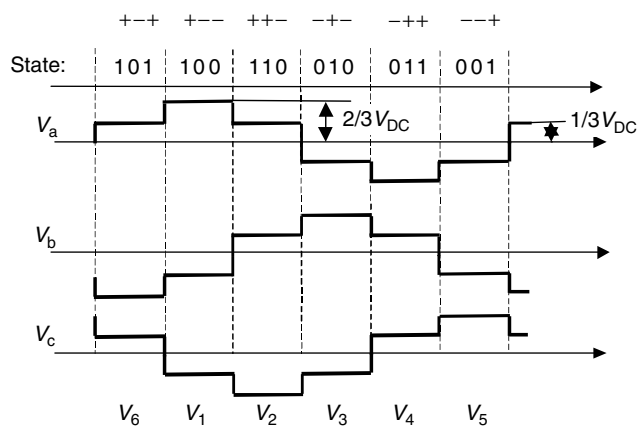**FIGURE 5.3** Basic topology for the three-phase voltage-source inverter.

FIGURE 5.4 Output voltage waveforms and state coding for a six-step operation.

Applying transform (Equation (5.2)) to these allows writing the same equations for the vector space variables.

$$v_s = L \frac{\mathrm{d}i_s}{\mathrm{d}t} \tag{5.13}$$

The variation slope of the phase current is doubled when the phase voltage gets doubled. The maximum value of the phase current is denoted here by I_M. During the time interval $[t_1, t_2]$, the output voltage vector is V_1 and the phase voltages are $2/3V_{\mathrm{dc}}$, $-1/3V_{\mathrm{dc}}$, and $-1/3V_{\mathrm{dc}}$.

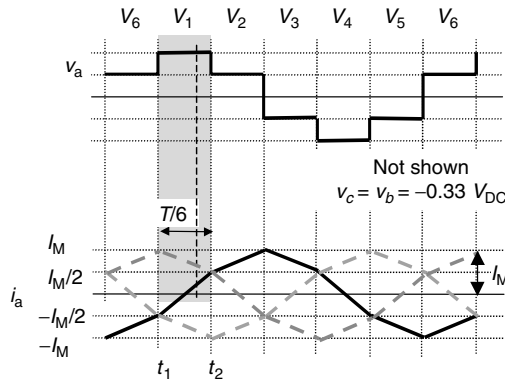**FIGURE 5.5** Switching vectors corresponding to the six-step operation of the inverter.

FIGURE 5.6 Output phase current and voltage waveforms.

Choosing the time origin in t_1 ($t_1 = 0$), the load current and voltage expressions can be mathematically expressed as linear variations during the interval (t_1, t_2). From Figure 5.6, this yields

$$
\begin{cases}
i_a(t) = -0.5I_M + \dfrac{2V_{DC}}{3L}t \\[2mm]
i_b(t) = -0.5I_M - \dfrac{V_{DC}}{3L}t \\[2mm]
i_c(t) = I_M - \dfrac{V_{DC}}{3L}t
\end{cases}
\tag{5.14}
$$

Applying definition (5.1) to the space vectors associated to the current and voltage waveforms yields

$$
v(t) = \frac{2}{3}[v_a(t) + av_b(t) + a^2v_c(t)]
\tag{5.15}
$$

$$
i(t) = \frac{2}{3}[i_a(t) + ai_b(t) + a^2i_c(t)]
\tag{5.16}
$$

where

$$
a = -\frac{1}{2} + j\frac{\sqrt{3}}{2} \qquad a^2 = -\frac{1}{2} - j\frac{\sqrt{3}}{2}
\tag{5.17}
$$

leading to

$$
v(t) = \frac{2}{3}V_d + j0
\tag{5.18}
$$

and

$$
i(t) = \left[-\frac{I_M}{2} + \frac{2}{3}\frac{V_d}{L}t \right] + j\left[-\frac{\sqrt{3}}{2}I_M \right]
\tag{5.19}
$$

It can be seen from Equation (5.18) that the magnitude of each voltage switching vector is $(2/3)V_{DC}$. The tip of the current space vector has a linear variation in the complex plane, with the *real* part varying linearly from $-0.5I_M$ to $0.5I_M$ during the time interval $[t_1, t_2]$ of duration $T/6$ (Figure 5.7). This trajectory is oriented so that the current space vector is quasi-perpendicular on the voltage space vector, and this is expected from the integral form of the inductive load equation. The vector projection on the *real* axis represents the value of the first phase current. The variation of the phase current during the interval $[t_1, t_2]$ allows determination of the maximum value of the current (I_M). It yields

$$\frac{2}{3}V_{DC} = L\frac{0.5I_M - (-0.5)I_M}{T/6} \tag{5.20}$$

and

$$I_M = \frac{2}{3L}\frac{T}{6}V_{DC} \tag{5.21}$$

The voltage space vector is identical with the switching vector V_2 at the next interval. The current space vector moves between the position along the vectors V_6 (at t_2) and V_1 (at next interval, t_3). Similar calculation proves the linearity of this trajectory. Extending the same reasoning for all six possible voltage-switching vectors defines the trajectory of the tip of the current vector in the complex plane. The resulting trajectory is a hexagon oriented along the voltage-switching vectors. The projection on the *real* axis is at any time equal to the current on the first phase. Currents or voltages on the other two phases can be graphically derived by the projection on two fictitious axes at 120 and 240° respectively. This vectorial analysis provides information about all the currents and voltages in the system. Moreover, because of the 60° symmetry of the operation, it is enough to limit the vectorial analysis to a 60° sector.

Extending this analysis to the general case of an R–L load, consider the vectorial equation for the load circuit

$$V_s = i_s R_s + L_s\frac{\mathrm{d}}{\mathrm{d}t}i_s \tag{5.22}$$

with the generic solution

$$i_s(t) = \frac{1}{R}V_s + Ce^{-t/\tau} \tag{5.23}$$

where C is a complex constant and $\tau = R/L$ represents the time constant of the load. In other words, for each switching vector applied to the load, the current trajectory is a portion of exponential (Figure 5.8). To better define such a trajectory, assume that the initial value is equal to $i(0) = I$ and the final value after $T/6$ is
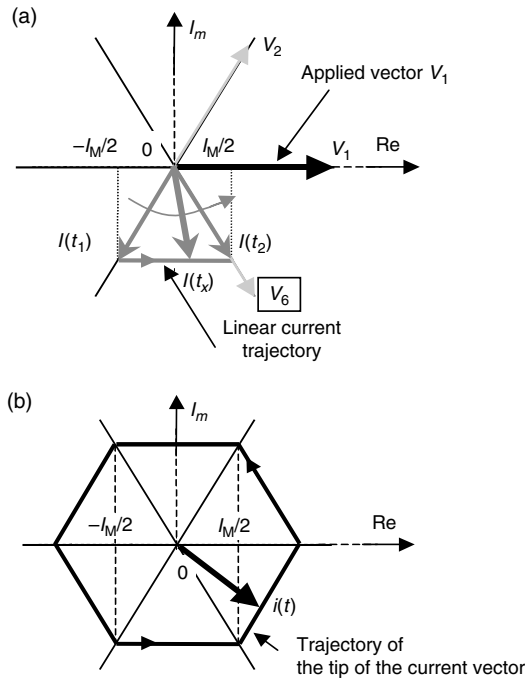
$$i\left[\frac{2\pi}{6\omega}\right] = Ie^{-j\pi/3}$$

FIGURE 5.7 Current vector trajectory in the complex plane for a pure L load. (a) Calculation, (b) full-cycle trajectory.

These conditions help to define the constant C and the initial value I:

$$\left.\begin{array}{l} t = 0 \Rightarrow I = \frac{1}{R}V_s + C \\ t = \frac{\pi}{3} \Rightarrow Ie^{j\pi/3} = \frac{1}{R}V_s + Ce^{-\pi/3\omega\tau} \end{array}\right\}$$

$$\Rightarrow \left\{\begin{array}{l} C = I - \frac{1}{R}V_s \\ Ie^{j\pi/3} = \frac{1}{R}V_s + Ce^{-\pi/3\omega\tau} \end{array}\right.$$

$$\Rightarrow \left\{\begin{array}{l} C = I - \frac{1}{R}V_s \\ Ie^{j\pi/3} = \frac{1}{R}V_s + \left(I - \frac{1}{R}V_s\right)e^{-\pi/3\omega\tau} \end{array}\right. \tag{5.24}$$

$$\Rightarrow \left\{\begin{array}{l} C = I - \frac{1}{R}V_s \\ I\left(e^{j\pi/3} - e^{-\pi/3\omega\tau}\right) = \frac{1}{R}V_s\left(1 - e^{-\pi/3\omega\tau}\right) \end{array}\right.$$

$$\Rightarrow \left\{\begin{array}{l} C = \frac{1}{R}V_s\left(\dfrac{1 - e^{-\pi/3\omega\tau}}{e^{j\pi/3} - e^{-\pi/3\omega\tau}} - 1\right) \\ I = \frac{1}{R}V_s\dfrac{1 - e^{-\pi/3\omega\tau}}{e^{j\pi/3} - e^{-\pi/3\omega\tau}} \end{array}\right.$$
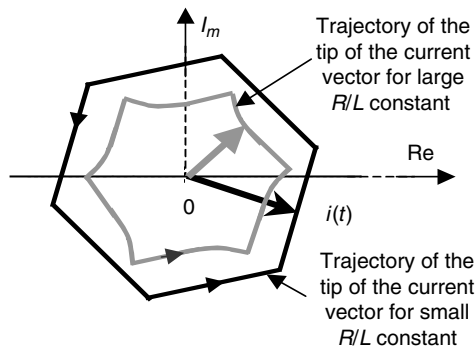
FIGURE 5.8 Current vector trajectory in the complex plane for an $R-L$ load.

Replacing complex constant C in Equation (5.23) yields

$$i(t) = \frac{1}{R} V_s \left[1 - e^{-t/\tau} \right] + I e^{-t/\tau} \qquad (5.25)$$

This gives a mathematical form to the expected exponential variation. If the inductive character is strong and τ is small, the trajectory is close to a hexagon in the complex plane. If the resistive term makes τ large enough, the trajectory suffers from the presence of the exponential term. Both cases are shown in Figure 5.8. The PWM operation splits this trajectory into smaller intervals of repetitive application of the switching vectors. The tip of the current vector follows a multi-edged trajectory, with each edge parallel to the same direction derived previously by the analysis of the six-step operation (Figure 5.9).

5.2.2 DEFINITION OF FLUX OF A (VOLTAGE) VECTOR AND IDEAL FLUX TRAJECTORY

Three-phase power-switching inverters are often used to supply a machine drive or a load strongly inductive. The leakage inductance of the machine and the inertia of the
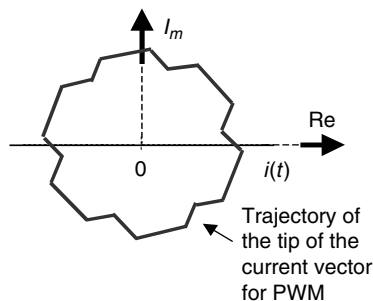

FIGURE 5.9 Current space vector trajectory for a simplified PWM case.

mechanical system account for low-pass filtering of the harmonics provided by the discontinuous power flow at switching. If a voltage drop across the resistance and leakage inductance of the stator windings is neglected, the flux linkage in the machine is approximately equal to the time integral of the impressed voltage. The flux vector yields

$$\lambda = \int V_s \, \mathrm{d}t \tag{5.26}$$

A very similar definition can be made for AC/DC applications, where the boost input inductance accounts for low-pass filtering of the voltage pulses resulting from the PWM operation of the power stage.

All these applications will work properly if the magnitude of the flux linkage is kept constant, which denotes a circular trajectory of the flux. As V_s occupies different discrete positions in the complex plane, its time integral leads to a polygon close to a circle, as anticipated by Figure 5.9. What was not explained previously is the existence of zero vectors in the flux trajectory at control with PWM. A zero vector, also called homopolar vector, is achieved when all power devices are connected to the same DC bus terminal, positive or negative. Any of the PWM methods explained previously in Chapter 3 uses zero-vector states during operation. Voltages applied on each phase of the load equal zero in this case and the integral of these voltages show no displacement of the flux trajectory. A direct consequence of this is the possibility of using zero vectors to regulate the speed of the flux trajectory (Figure 5.10).

A real trajectory of the flux achieved by PWM operation presents both radial and angular errors. The radial errors are variations along the radius of the circular locus, whereas the angular errors are variations from a constant rotational speed. In a motor
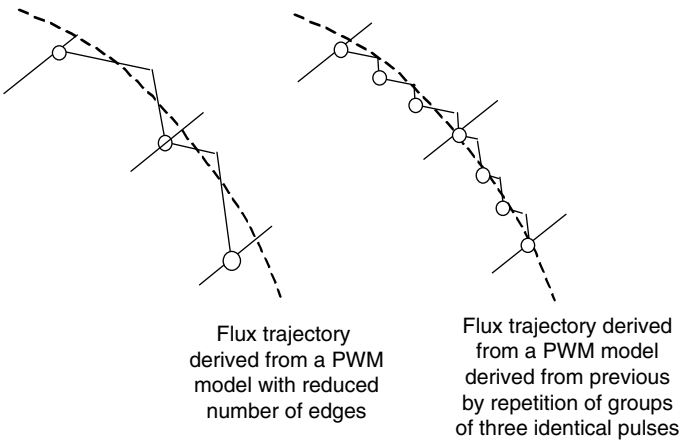

Flux trajectory derived from a PWM model with reduced number of edges

Flux trajectory derived from a PWM model derived from previous by repetition of groups of three identical pulses

FIGURE 5.10 Flux trajectory improved by increasing the switching frequency even if the same shape of pulses is used.

drive, any error in the flux trajectory has a direct influence on the torque ripple. The difference between the reference λ_0 having a circular locus in the complex plane and the actual trajectory λ produced by a PWM inverter causes the torque oscillations.

The dependence of the torque pulsation on radial and angular components of the flux error has been analyzed and presented in [13–17], and it has been stated that the torque oscillation is more sensitive to the angular error than the radial error. The angular error can be reduced by operating with a smoother rotational speed that can be achieved when employing more zero states on the flux locus. The radial errors can be reduced with an optimal polygonal flux locus having all edges staying as close to the desired circular locus.

As the angular error is more important than the radial error, the torque ripple is lower when a higher carrier frequency (more zero vector states) is employed, even though this splits a polygonal flux locus to a reduced number of edges. A limited switching frequency is desired for completely different reasons, such as reduction of the switching loss.

5.3 SVM THEORY: DERIVATION OF THE TIME INTERVALS ASSOCIATED TO THE ACTIVE AND ZERO STATES BY AVERAGING

SVM was developed in [7–11] and the importance of this method has been outlined in many publications [18–21]. The three-phase inverter presented in Figure 5.3 produces a symmetrical three-phase system of voltages on the load. If the magnitude of the phase voltages is V_s, this is equivalent to generating a circular locus with a constant radius equaling the same magnitude. Such an ideal locus cannot be achieved with a switching power converter that leads to six discrete positions of only the voltage space vector. Each desired position on the circular locus can be synthesized only through an average relationship between two neighboring active vectors and zero vectors

$$V_s T_s = V_a t_a + V_b t_b + V_0 t_0 \qquad (5.27)$$

where T_s is the sampling period of the given circular locus (as, usually, the switching frequency is not equal to the carrier frequency, it is preferable to call T_s the sampling period) and t_a, t_b are the time intervals allocated to the neighboring vectors V_a, V_b. The averaging process is a result of the low pass filtering action of the load on the voltage pulses. Zero vectors are necessary to keep the sampling interval constant and they are calculated by

$$t_0 = T_s - t_b - t_a \qquad (5.28)$$

In order to calculate the time intervals associated with a desired position of the voltage vector in the complex plane, the symmetry after a $60°$ interval is first noticed. This opens up the possibility that the analysis can be limited to a generalized sector of $60°$, repeated six times. To simplify the calculation, such a sector is considered superimposed with the first sector of the complex plane.

Decomposition of Equation (5.27) on *real* and *imaginary* axes yields:

$$\begin{cases} \text{Re: } V_s \cos \alpha T_s = \left(\frac{2}{3}V_{DC}\right) t_a + \left(\frac{2}{3}V_{DC}\right)\frac{1}{2}t_b \\ \text{Im: } V_s \sin \alpha T_s = \left(\frac{2}{3}V_{DC}\right)\frac{\sqrt{3}}{2}t_b \end{cases} \tag{5.29}$$

Time intervals involved in the PWM generation are calculated by (Figure 5.14):

$$\begin{cases} t_a = \frac{3V_s}{2V_{DC}}T_s\left(\cos \alpha - \frac{1}{\sqrt{3}}\sin \alpha\right) = \frac{\sqrt{3}V_s}{V_{dc}} T_s \sin\left[\frac{\pi}{3} - \alpha\right] \\ t_b = \frac{\sqrt{3}V_s}{V_{DC}}T_s \sin \alpha \\ t_0 = T_s - t_a - t_b \end{cases} \tag{5.30}$$

Calculation of the time intervals associated with each active state is only the first part of the generation of a PWM algorithm. Determination of the switching sequence is the second stage. Modern microcontrollers achieve both functions and take advantage of special expressions for the time intervals associated with the conduction of each switch. These allow the implementation of the SVM method within the center-aligned PWM hardware. Calculation of the pulse widths is based on a memory look-up table for the sine function within a $60°$ interval or of the $\sin \alpha$ and $\sin (60 - \alpha)$ functions within a $30°$ interval. Alternative solutions are based on real-time interpolation of a minimized look-up table. This interpolation can be carried out by *fuzzy logic* as well [22,23]. Chapter 9 will present hardware solutions available in the market to implement SVM.

Observing Equation (5.30) and Figure 5.11, one can derive the maximum modulation. It will correspond to the circular locus with the maximum radius and it equals

$$V_{max} = \frac{2}{3}V_{DC} \cos\frac{\pi}{6} = \frac{1}{\sqrt{3}}V_{DC} = 0.577V_{DC} = 0.866 \left[\frac{2V_{DC}}{3}\right]$$

$$m_{max} \xrightarrow{\text{definition}} \frac{V_{max}}{V_{magn\_six\_step}} \Rightarrow m_{max} = 0.866 \tag{5.31}$$

This value is 15% higher than the maximum modulation index from the sinusoidal modulation.

The sampling period T_s is shown in Equation (5.30). Note the nomenclature difference between sampling interval/sampling frequency and switching interval/switching frequency. A new PWM method can be derived by changing the sampling frequency while using the same equations. The frequency modulation is the result of adjusting T_s during the fundamental or cycle period [10,17]. Several methods have been developed by using the sampling frequency as a degree of freedom in optimization after one or more criteria: low harmonics reduction, harmonic current factor
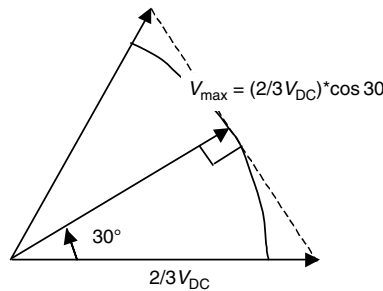
$V_{max} = (2/3\,V_{DC})^*\cos 30$

$30°$

$2/3\,V_{DC}$

FIGURE 5.11 Definition of the maximum modulation index. (From Neacsu DO, Tutorial presented at IECON'01: The 27th Annual Conference of the IEEE Industrial Electronics Society 2001, IEEE Paper 0-7803-7108-9/01. With permission.)

(HCF) reduction, and so on, but all redefine T_s as

$$T_s = \frac{1}{Nf}(1 + \delta\cos(6\alpha)) \tag{5.32}$$

with N being number of intervals over the fundamental period (at frequency f).

Conventional PWM is characterized by $\delta = 0$, while the optimized methods require T_s modulated so that it gets shorter periods at 0 and $60°$ but lengthier at $30°$ within each $60°$ sector. These ensure minimum angular errors, current distortion factor at low harmonics, and minimum torque oscillations. Random SVM represents a special type of frequency modulation.

Finally, note that the averaging principle used here does not provide any requirement on zero vector generation during t_0. Moreover, the sequence of the active and zero vectors within the sampling period is not unique and these degrees of freedom make the difference between space vector methods. The most well-known alternatives will be analyzed later in this chapter.

5.4 ADAPTIVE SVM: DC RIPPLE COMPENSATION

The presence of the DC voltage (V_{DC}) in Equation (5.30) compensates for the ripple of the DC bus voltage [24] (Figure 5.12). This ripple can be produced with insufficient filtering of the input rectifier power stage in a back-to-back converter structure. Measuring the DC voltage at each sampling interval or with a larger sampling period will be appropriately compensated by Equation (5.30) for the effect of this ripple in the output voltage.

Figure 5.13 shows how the time intervals t_a, t_b are affected by the variation of the DC bus voltage in order to preserve the same harmonics on the load. The drawback of this method is that it reduces the maximum available voltage at the inverter output. The maximum available output voltage is achieved when the DC bus has the lower value within the ripple and the inverter operates at maximum modulation index of 0.866.
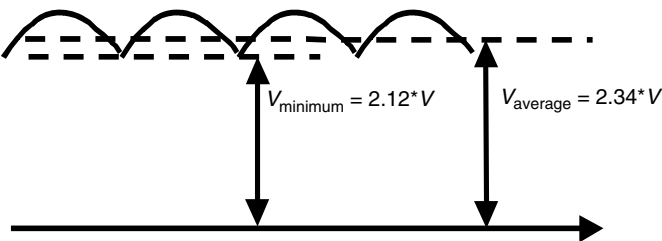
FIGURE 5.12 Reduction of the maximum output voltage by an unfiltered DC bus with a six-step rectifier.

5.5 LINK TO VECTOR CONTROL: DIFFERENT FORMS AND EXPRESSIONS OF TIME INTERVAL EQUATIONS IN THE (*d,q*) COORDINATE SYSTEM

This SVM algorithm calculates the time intervals associated with each state based on the polar coordinates (V_s, α) of the desired space vector position. This is not very convenient for vector control methods for drives and for active filtering.

The result of the vector control methods is given in the coordinates (v_x, v_y) and these can also be expressed depending upon the polar coordinates (5.33 to 5.38) [25].

Sector 1

$$v_x = V_s \cos \alpha$$
$$v_y = V_s \sin \alpha \tag{5.33}$$

Sector 2

$$v_x = V_s \cos\left[\alpha + \frac{\pi}{3}\right]$$
$$v_y = V_s \sin\left[\alpha + \frac{\pi}{3}\right] \tag{5.34}$$

FIGURE 5.13 SVM with adaptive compensation.

Sector 3

$$v_x = -V_s \cos\left[\frac{\pi}{3} - \alpha\right]$$
$$v_y = V_s \sin\left[\frac{\pi}{3} - \alpha\right]$$

(5.35)

Sector 4

$$v_x = -V_s \cos\alpha$$
$$v_y = -V_s \sin\alpha$$

(5.36)

Sector 5

$$v_x = -V_s \cos\left[\alpha + \frac{\pi}{3}\right]$$
$$v_y = -V_s \sin\left[\alpha + \frac{\pi}{3}\right]$$

(5.37)

Sector 6

$$v_x = V_s \cos\left[\frac{\pi}{3} - \alpha\right]$$
$$v_y = -V_s \sin\left[\frac{\pi}{3} - \alpha\right]$$

(5.38)

For the first sector, replacing Equation (5.33) in Equation (5.30) yields

$$\begin{cases} t_a = \dfrac{3}{2\,V_{DC}}T_s\left(v_x - \dfrac{1}{\sqrt{3}}v_y\right) \\ t_b = \dfrac{\sqrt{3}}{V_{DC}}T_s v_y \\ t_0 = T_s - t_a - t_b \end{cases}$$

(5.39)

For the second sector

$$\begin{cases} v_x = V_s\left[\cos\alpha\dfrac{1}{2} - \sin\alpha\dfrac{\sqrt{3}}{2}\right] \\ v_y = V_s\left[\sin\alpha\dfrac{1}{2} + \cos\alpha\dfrac{\sqrt{3}}{2}\right] \end{cases} \Longrightarrow \begin{cases} \sin\alpha = \dfrac{1}{2}\dfrac{v_y}{V_s} - \dfrac{\sqrt{3}}{2}\dfrac{v_x}{V_s} \\ \cos\alpha = \dfrac{1}{2}\dfrac{v_x}{V_s} + \dfrac{\sqrt{3}}{2}\dfrac{v_y}{V_s} \end{cases}$$

$$\Longrightarrow \begin{cases} t_a = \dfrac{3}{2V_{DC}}T_s\left(v_x + \dfrac{1}{\sqrt{3}}v_y\right) \\ t_b = \dfrac{\sqrt{3}}{V_{DC}}T_s\left(\dfrac{1}{2}v_y - \dfrac{\sqrt{3}}{2}v_x\right) \end{cases}$$

(5.40)

Similar calculus leads to the following results [25]:

Sector 1

$$t_a = \frac{3T_s}{2V_{DC}}\left(v_x - \frac{1}{\sqrt{3}}v_y\right)$$

$$t_b = \frac{\sqrt{3}T_s}{V_{DC}}v_y$$

(5.41)

Sector 2

$$t_a = \frac{3T_s}{2V_{DC}}\left(v_x + \frac{1}{\sqrt{3}}v_y\right)$$

$$t_b = \frac{\sqrt{3}T_s}{V_{DC}}\left(\frac{1}{2}v_y - \frac{\sqrt{3}}{2}v_x\right)$$

(5.42)

Sector 3

$$t_a = \frac{T_s\sqrt{3}}{V_{DC}}(v_y)$$

$$t_b = \frac{\sqrt{3}T_s}{2V_{DC}}(-v_y - \sqrt{3}v_x)$$

(5.43)

Sector 4

$$t_a = \frac{3T_s}{2V_{DC}}\left(-v_x + \frac{1}{\sqrt{3}}v_y\right)$$

$$t_b = \frac{-\sqrt{3}T_s}{V_{DC}}v_y$$

(5.44)

Sector 5

$$t_a = \frac{\sqrt{3}T_s}{2V_{DC}}(-v_x - 2v_y)$$

$$t_b = \frac{\sqrt{3}T_s}{2V_{DC}}(-v_y + v_x)$$

(5.45)

Sector 6

$$t_a = \frac{3T_s}{2V_{DC}}\left(v_x - \frac{2\sqrt{3}}{3}v_y\right)$$

$$t_b = \frac{\sqrt{3}T_s}{2V_{DC}}(v_y - \sqrt{3}v_x)$$

(5.46)

The time intervals allocated to the zero vectors remain

$$t_0 = T_s - t_a - t_b$$

(5.47)

Another mathematical form for the transformation of (v_x, v_y) coordinates into time intervals is provided by Equation (5.48) and is derived from (x, y)-type orthogonal coordinates of the active switching vectors denoted here as (V_x^2, V_y^2) and (V_x^1, V_y^1). The relationship for the time intervals yields

$$
\begin{aligned}
t_1 &= \frac{[V_y^2 v_x - V_x^2 v_y] T_s}{V_x^1 V_y^2 - V_x^2 V_y^1} \\
t_2 &= \frac{[V_x^1 v_y - V_y^1 v_x] T_s}{V_x^1 V_y^2 - V_x^2 V_y^1}
\end{aligned}
\tag{5.48}
$$

Any of these forms expressing the time intervals represents only the first step for PWM implementation. Next, the time intervals corresponding to the inverter-switching states need to be converted into a logical switching sequence applied to the gates of IGBTs. In order to implement this step, the *switching reference function* (also called *modulation function*) is defined.

5.6   DEFINITION OF THE SWITCHING REFERENCE FUNCTION

Once we know the time intervals for each state, we need to establish the sequence of these intervals. If we try to directly use the previous relationships, the definition of the switching sequence can be implemented only by the software. It is more advantageous to define a function called the *switching reference function* that represents the duty ratio of each inverter leg or the conduction time normalized to the sampling period for a given switch; this is a mathematical function varying between 0 and 1 centered around 0.5. This is also called the *modulation function*.

The switching reference function can be derived by algebraic operations between the time intervals previously calculated. For instance, on the first sector from Figure 5.14:

- The instant when S1 goes ON equals t_{01} from the beginning of the sampling period, and the value of the switching reference function for S1 will equal $[t_{01}/T_s]$.
- The instant when S3 goes ON equals a delay of $t_{01} + t_a$ from the beginning of the sampling period, and the value of the switching reference function for S3 will equal $[t_{01} + t_a/T_s]$.
- The instant when S5 goes ON equals a delay of $t_{01} + t_a + t_b$ from the beginning of the sampling period, and the value of the switching reference function for S5 will equal $[t_{01} + t_a/T_s]$.

The switching reference function is calculated at the sampling instants, and the real variation is a staircase waveform that can be interpolated as shown in Figure 5.13. The switching reference function has the same meaning as the reference used in sine-triangle comparison-based PWM methods. It is, therefore, simpler to
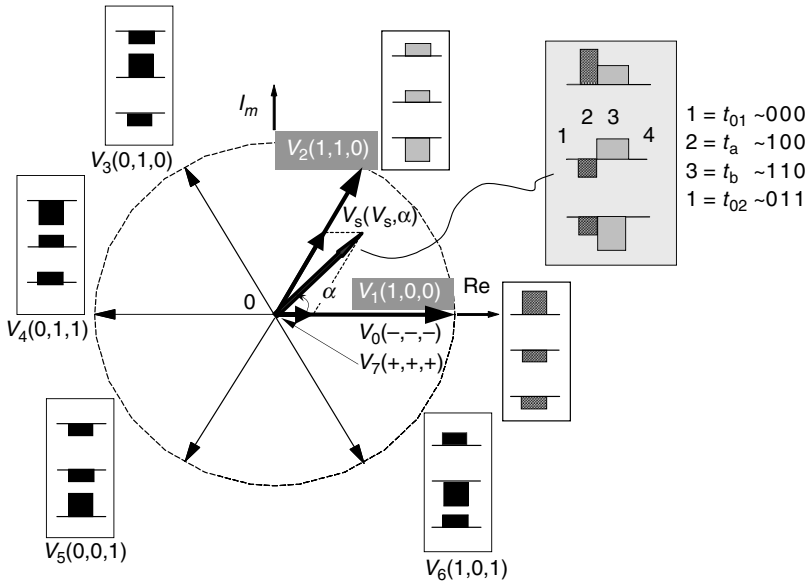
FIGURE 5.14 Generation of voltage space vector by SVM. (From Neacsu DO, Tutorial presented at IECON'01: The 27th Annual Conference of the IEEE Industrial Electronics Society 2001, IEEE paper 0-7803-7108-9/01. With permission.)

use the mathematical definition of a continuous function not influenced by the sampling frequency rate. At this point, it is also easier to understand why the repetitive frequency used in PWM generation is called sampling frequency. It simply means to sample the switching reference function.

After successive derivations from Equation (5.38) through Equation (5.43), one can calculate the switching reference function for all sectors. This is shown in Figure 5.15 for the case of regular SVM. The difference between this function and a pure cosine function is given by the following equation with a rich content in the third harmonic:

$$PW_{harm} = \begin{cases} 0.500 \sin \alpha, & \text{for } \alpha \in (0,60) \\ 0.866 \cos \alpha, & \text{for } \alpha \in (60,120) \\ -0.500 \sin \alpha, & \text{for } \alpha \in (120,180) \end{cases} \tag{5.49}$$

The third harmonic is present in the switching reference function but it is not present in the output phase or line voltages. It only represents the average of the A–M voltage from Figure 5.16:

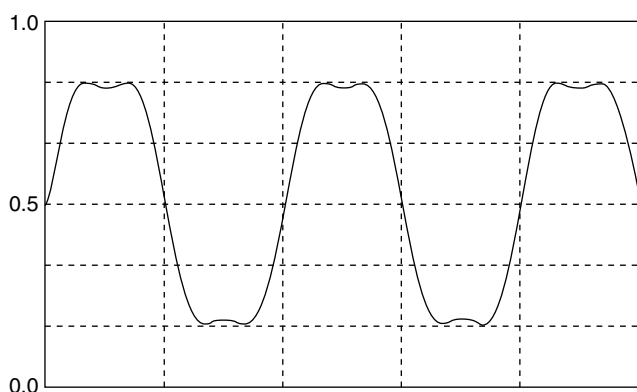$$v_{AB} = v_{AM} - v_{BM} \implies \text{third harmonic vanishes} \tag{5.50}$$

FIGURE 5.15 Switching reference function for the regular SVM. (From Neacsu DO, Tutorial presented at IECON'01: The 27th Annual Conference of the IEEE Industrial Electronics Society 2001, IEEE Paper 0-7803-7108-9/01. With permission.)

The previous chapter showed the role and meaning of the injection of the third harmonics in the sinusoidal modulation. The amount of this harmonic injection has been shown to vary depending on the optimization objective:

- Maximization of the fundamental content (third harmonic with 0.25 of the magnitude of the sinusoidal reference)
- Minimization of the total content in harmonics (third harmonic with 0.16 of the magnitude of the sinusoidal reference)

The third harmonic in the SVM method is between the two values previously calculated at about 0.22. References [27–30] analyze the equivalence between regular, sampled sine-triangle methods and SVM and conclude that both methods are analogous and that conventional digital center-aligned PWM devices can be used for the implementation of the SVM algorithm.
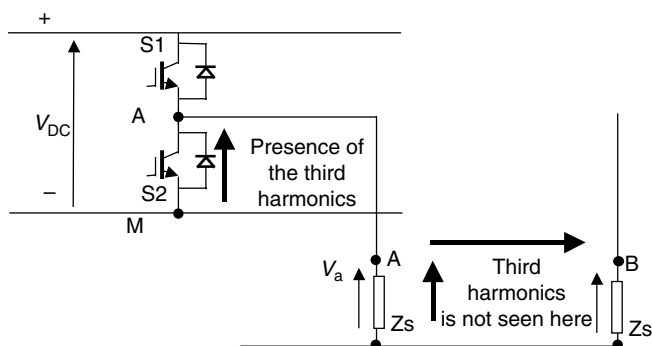

FIGURE 5.16 Third harmonics in SVM generation.

5.7 DEFINITION OF THE SWITCHING SEQUENCE

5.7.1 CONTINUOUS REFERENCE FUNCTION: DIFFERENT METHODS

5.7.1.1 Direct-Inverse SVM [9,11]

The number of switchings can be reduced with a special arrangement of the switching sequence so that only one switching on each inverter leg occurs during the transition from one state to the next. When using both available zero states from Figure 5.14, one zero state will start the sequence and the other will end it. For instance, the switching state sequence has to be $\cdots 0\ 1\ 2\ 7\ 2\ 1\ 0\cdots$ The only remaining degree of freedom consists in the amount t_0 shared between the vectors V_0 and V_7.

The averaging theory used for SVM calculation does not define a way of sharing t_0 among the possible zero vector states. In the original method, t_0 was shared equally between the two zero vectors. But this is not the most optimal partition solution. The same low-sampling frequency algorithm is analyzed but with different sharing of the zero states. All the sectors and bisectrix symmetries are considered as well as the alternation of the zero state vectors. Results for the sharing ratio are shown in Figure 5.17 and Figure 5.18 for a low number (equal to 24) of sampling intervals in the fundamental [31,32]. At larger sampling frequencies, the differences are smaller.

These results also show that high-performance SVM systems can be improved further by a different placement of the zero states within the sampling interval.

The two extreme situations for the sharing of the zero-state intervals are:

- Method D-I-H (direct-inverse-half) (Figure 5.19, Figure 5.21a): Equal sharing of the zero vector intervals at each sampling interval ($t_0 = t_7$) [10,11] is shown in Figure 5.19 with a phase voltage waveform. Observe the trajectory of the tip of the current vector derived from this sequence.
- Method D-I-O (direct-inverse-one) (Figure 5.20): Use of only a zero vector interval within each sampling period (e.g., $t_0 = 0$, $t_7 = T_s - t_a - t_b$).
- Both methods determine three switching on each sampling periods. Method D-I-O is often employed at high sampling frequencies, whereas in low
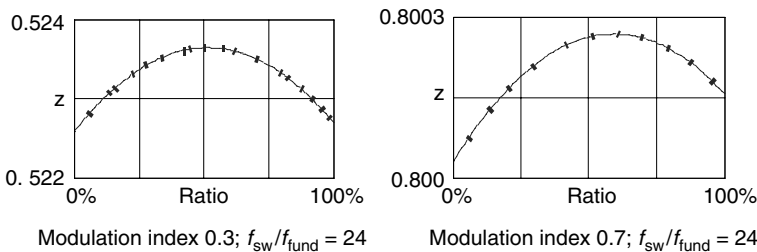

FIGURE 5.17 Effect of different sharing of the zero state interval in the content of fundamental (z). (From Neacsu DO, Tutorial presented at IECON'01: The 27th Annual Conference of the IEEE Industrial Electronics Society 2001, IEEE Paper 0-7803-7108-9/01. With permission.)
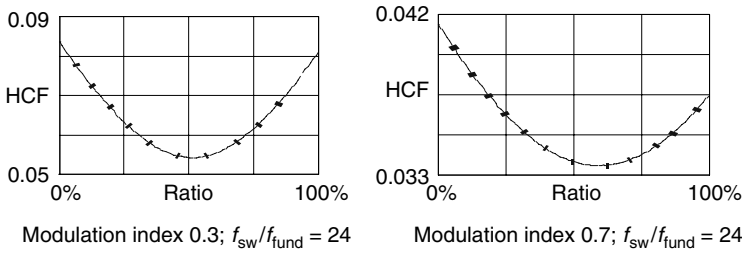
FIGURE 5.18 Effect of different sharing of the zero state interval in HCF. (From Neacsu DO, Tutorial presented at IECON'01: The 27th Annual Conference of the IEEE Industrial Electronics Society 2001, IEEE Paper 0-7803-7108-9/01. With permission.)

frequencies, it produces even harmonics in the output phase voltage, as the waveform symmetries are no longer taken into account. The spectral differences between the voltages carried out by either Method D-I-H or Method D-I-O are small if the sampling frequency is large enough.

- Simple direct SVM or S-D-H Method: The simplest way to synthesize the output voltage vector is to turn on all the switches connected to the same DC link potential at the beginning of the switching cycle (sampling period) and to turn them off sequentially during the sampling interval. The zero-vector interval splits between V_0 and V_7 ($t_0 = t_7$). The drawback consists in switching all three inverter legs somewhere in the middle of the sampling interval in order to change from V_0 to V_7 (for instance, the switch sequence: $\cdots 0127 - 0127 - 0127 \cdots$). This method is similar to the usual sine-triangle comparison-based PWM (Figure 5.28, Figure 5.2b).

- Symmetrically generated SVM: This modulation scheme is based on a symmetrical sequence within each sampling period. The phase voltages and switching signals are similar to the D-I-H method but the direct-inverse sequence is now inside the same sampling period (Figure 5.36). This method is similar to the center-aligned PWM devices and can be directly implemented in the existing PWM IC working on this basis.
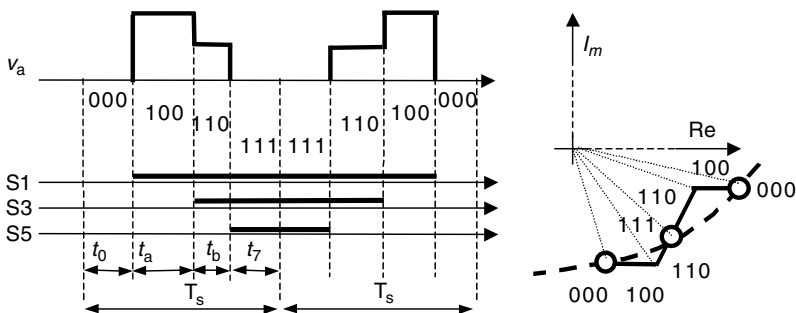

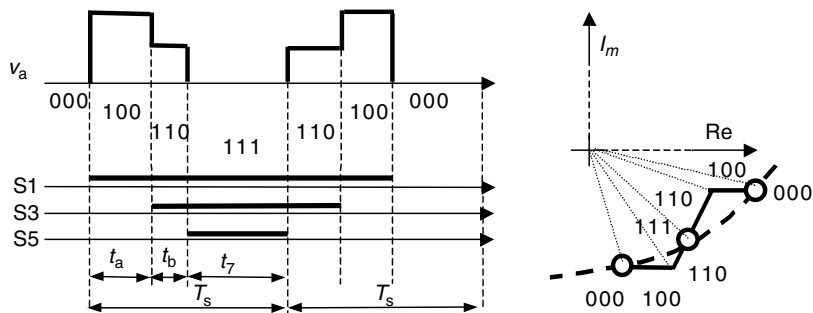**FIGURE 5.19** Pulse generation with method D-I-H.

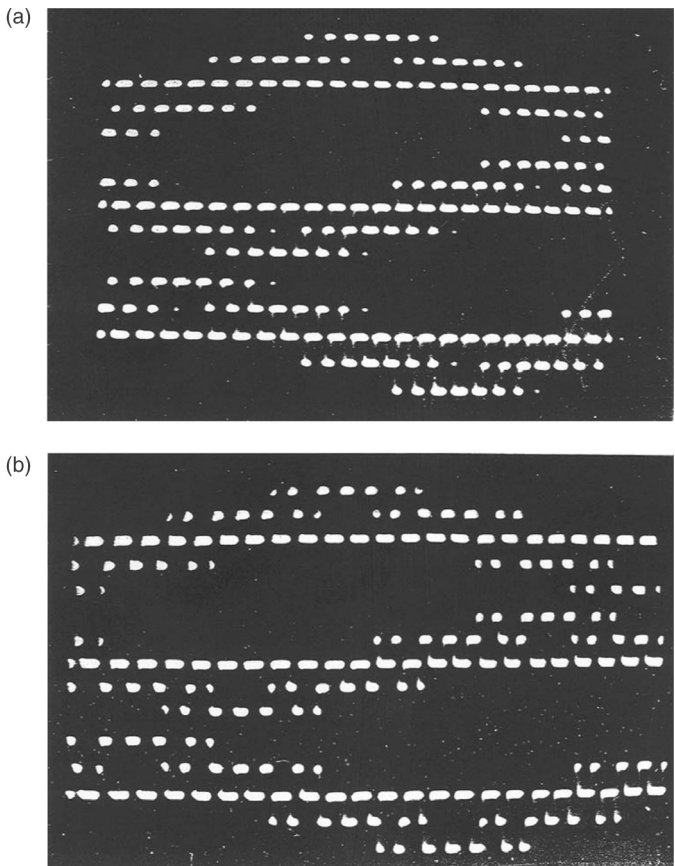**FIGURE 5.20** Pulse generation with method D-I-O.

(a)

(b)

FIGURE 5.21 Three-phase voltage waveforms for (a) direct inverse and (b) direct sequences at a low-sampling frequency.

5.7.2 Discontinuous Reference Function [33–42] for Reduced Switching Loss

The previous chapter including the regular sampled PWM algorithms, demonstrated the advantages of discontinuous algorithms to reduce the inverter switching loss [33–37]. The same idea is now used with the SVM algorithm as support [38–42].

The averaging theory used for SVM calculation does not define the sequence of the switching states. Any possible sequence of states will satisfy the average relationship if the time intervals are calculated correctly. Any two neighboring vectors are different by only one a switching in an inverter leg. Therefore, always select the zero vector that does not change the status of that zero vector. For instance, in the first sector, shown in Figure 5.14, the first leg does not switch when active vectors are changed (from 1 0 0 to 1 1 0 or vice versa). Selection of the homopolar vector is not unique; each time two zero vectors can be used. Always selecting 1 1 1 as the zero vector means that the first leg will not switch for the whole first sector (for instance, sequences $\cdots-1\ 1\ 1-1\ 1\ 0-1\ 0\ 0-1\ 1\ 1-1\ 1\ 0-1\ 0\ 0-1\ 1\ 1-\cdots$). But this solution is not unique. In the first sector, the third leg does not switch when the active vectors are changed. This time, the lower switch will be ON during both active states (from 1 0 0 to 1 1 0 or vice versa). Always selecting 0 0 0 as the zero vector means that the third leg will not switch for the whole first sector (for instance, sequences $\cdots-0\ 0\ 0-1\ 0\ 0-1\ 1\ 0-0\ 0\ 0-1\ 0\ 0-1\ 1\ 0-0\ 0\ 0\cdots$). The advantage of using any one of these solutions is the reduction in switching losses. There are two solutions to minimize the number of switching processes within each sector of the complex plane. This raises the question whether to change or not the selection of the zero vector and the whole optimized sequence when passing to the next sector.

If we do not ever change the selection of the zero vector and always select the zero vector as 0 0 0 or 1 1 1, we get one of the following solutions:

- *Method DZ0*: The null vector is always fixed as [0 0 0]
- *Method DZ1*: The null vector is always fixed as [1 1 1]

The switching reference function can be calculated as shown previously in section 5.5 and it leads to the waveforms shown in Figure 5.22, with large intervals that have no switchings for each of the six IGBTs within the inverter. These functions are also not linear.

As can be seen, the switch that is not switched is either always on the low-side (for the selection of the 0 0 0 zero vector) or on the high-side (for the selection of the 1 1 1 zero vector). Three switches are ON for extended periods of time and this may create a problem in inverter bridges that use isolation circuits such as the *bootstrap* or *charge pumps* for their gate drivers. That is why these methods are not used in the industry.

To obtain a symmetrical stress from the power devices, the degree of freedom consists in alternating the zero vector at each 60° interval. As each phase can be kept unswitched for 120° consecutively, there is a degree of freedom in selecting where exactly the zero vector can be changed for sequences of 60°. For instance, the first leg can be kept unswitched from −60 to 60° (notice vectors 1 1 0 and
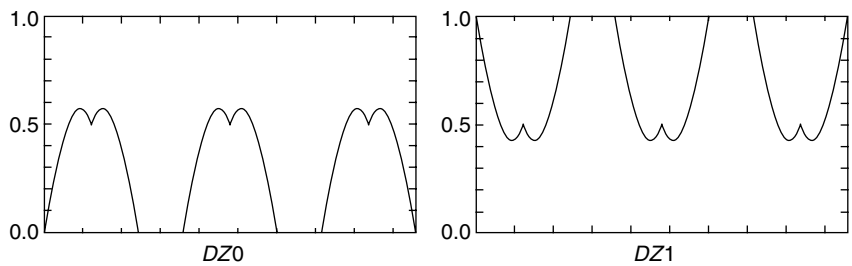
FIGURE 5.22 Switching reference function calculated for PWM generation with methods DZ0 and DZ1.

1 0 0 in Sector 1; 1 0 0 and 1 0 1 in Sector 6), but a 60° interval has to be chosen within this. Switching loss is approximately proportional to the magnitude of the current being switched and it would be better to avoid switching the inverter leg with the highest instantaneous current. In other words, the no-switching 60° interval can be selected at exactly the peak of the current.

How is the switching sequence selected? It can be based on four states in each sampling interval: a zero vector in the beginning, the first active state, the second active state, and another zero state at the end. Applying the principles explained earlier to such a switching sequence leads to results shown in Figure 5.23. The same phase voltages are obtained as in the case of Method S-D-H.

However, such a sequence violates the idea of having only one switch at a time and leads to four switches over a sampling interval. Another solution that respects this constraint and also takes advantage of the no-switch rule for 60° consecutively is different from conventional SVM. It uses a direct-inverse sequence $|V_{A1} - V_{A2} - V_Z| V_Z - V_{A2} - V_{A1} | V_{A1} - V_{A2} - V_Z |$ (Figure 5.37).

This selection of the switching sequence allows the maximum reduction of the number of switches.
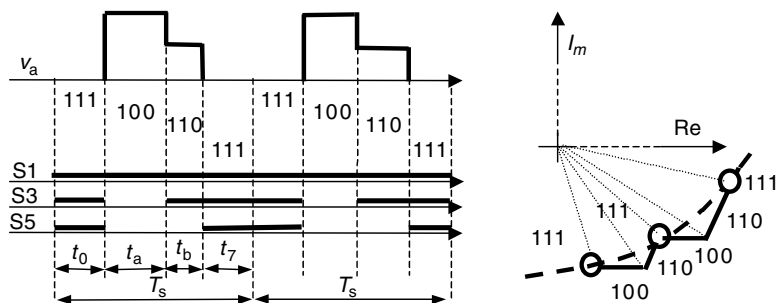

FIGURE 5.23 Switching sequence with four states take advantage of no-switch rule on the first leg.

There are several solutions accepted by the industry:

- Method DD1: The intervals of no switches coincide with the plane sectors. A null vector [1 1 1] is assigned for sectors 1, 3, and 5 and a null vector [0 0 0] is assigned for sectors 2, 4, and 6. The 60° interval without switches occurs right after the peak of the phase voltage. Generally, the current lags behind the phase voltage and the peak of the current fundamental settles in the next 60° after the peak voltage (Figure 5.38).
- Method DD2: The 60° no-switch interval is spread equally around the peak of the fundamental of voltage. This method is very useful to reduce switching losses in grid-related applications, in which the power factor is unity and the peak of current is close to the peak of voltage (Figure 5.38).
- Method DD3: The 60° interval without switches can be spread equally around the measured peak of the phase current. Despite the difficulty of sensing the phase currents, this solution seems attractive, as it tracks the maximum loss reduction. However, if the phase current and voltage out of phase are greater than 30°, the 60° no-switch region will overcome the vector sector (Figure 5.24).

If the voltage vector is, for instance, V_1 and the current vector is at 48°, equally spreading the no-switch region for the first inverter leg around the current vector leads to an area between 18 and 78°. For $\alpha > 60$, keeping the first phase ON (1) is no longer possible as the Sector 2 is characterized by switches in the first phase due to the use of $V_3(0\ 1\ 0)$. There need not be any switches in the other two phases, but the other currents are less able to control the complexity, thereby compromising the merits of the method.

Let us analyze Figure 5.25 to understand how much power loss can be saved by using discontinuous PWM algorithms. Switching power loss for the discontinuous
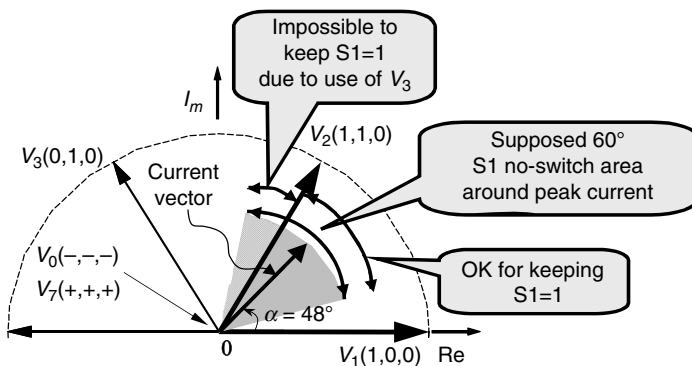

FIGURE 5.24 Vectorial discussion around the DD3 method. (From Neacsu DO, Tutorial presented at IECON'01: The 27th Annual Conference of the IEEE Industrial Electronics Society 2001, IEEE Paper 0-7803-7108-9/01. With permission.)
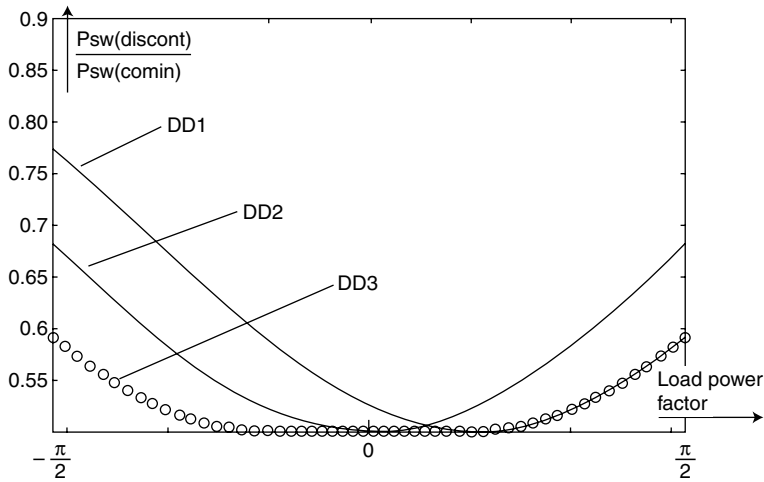
FIGURE 5.25 Switching loss for discontinuous PWM normalized to the switching loss for continuous PWM algorithm versus load power angle. (From Neacsu DO, The 27th Annual Conference of the IEEE Industrial Electronics Society 2001, IEEE Paper 0-7803-7108-9/01. With permission.)

PWM algorithm is normalized to the switching power loss for the continuous PWM algorithm and shown in respect with the load power angle. The results are based on a computer-based analysis, considering the level of the load current at switching instant and the number of switching processes. The best case leads to 50% savings in switching loss [42–44].

This reduction in switching loss does not exactly come free. There is a small drawback as the discontinuous PWM methods can introduce oscillations around the points where the sector is changed. This is due to the different set of equations used within each sector to calculate the time intervals. The effects are clearer at low output fundamental frequencies and they result in increased loss in the load and may introduce instabilities of the feedback control system (Figure 5.26).

5.8 COMPARISON BETWEEN DIFFERENT VECTORIAL PWM

5.8.1 LOSS PERFORMANCE

The difference between the conduction loss among the SVM techniques is less than 3% of the total loss. Switching performance is presented in Table 5.1.

5.8.2 COMPARISON OF TOTAL HARMONIC DISTORTION/HCF

As shown in the previous chapter, the most important performance index for a power converter refers to the harmonic content in the output (input) current. This can be
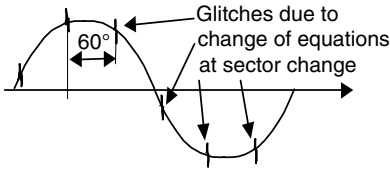
FIGURE 5.26 Output phase current when applying discontinuous PWM algorithms.

expressed by

$$HCF(\%) = \frac{100}{V_{(1)}} \sqrt{\sum_{n=5}^{\infty} \left[\frac{V_{(n)}}{n}\right]^2} \tag{5.51}$$

and represents a normalization of the harmonic content to the fundamental.

These PWM algorithms have different sequences during the sampling interval and the number of switching processes is different. For this reason, the definition of the switching frequency differs from method to method. A proper comparison must consider the same switching frequency even if reached by different means.

The best harmonic content is achieved for reduced loss algorithm operated at high-modulation indices. In low-modulation indices, the best harmonic content can be achieved from the conventional SVM. The approximate *threshold* for this kind of comparison lies at a modulation index of about 0.6.

Many other researchers or engineers present the current harmonic by normalization to the harmonics obtained by a six-step operation at the power stage. Figure 5.39 shows the difference between harmonics with an inverter obtained by a six-step operation and a PWM inverter. The operation with six pulses introduces larger harmonics at low frequency.

TABLE 5.1
Switching Performance

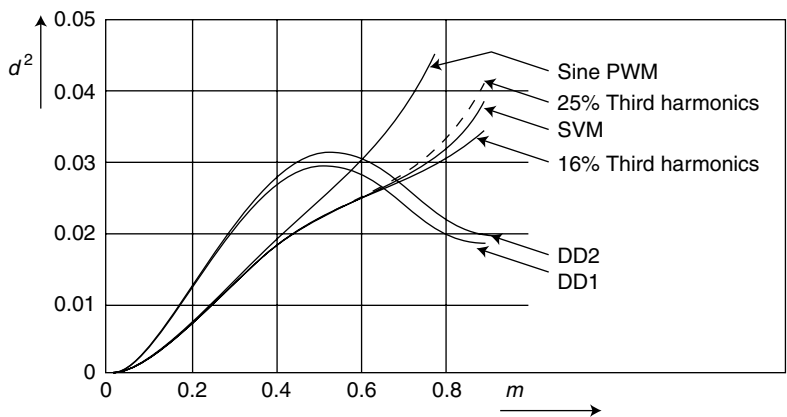| Method	Number of Switchings Within T_s	THDv	Number of Switching States
Direct-inverse (D-I-H)	3		4
Direct inverse (D-I-O)	3		3
Simple direct (S-D-H)	6		4
Symmetrically generated (SGS)	6	Least	7
Direct-direct/000 (DZ0)	4		3
Direct-direct/111 (DZ1)	4		3
Direct-direct/sect (DD1)	4/2		3
Direct-direct/peak (DD2)	4/2		3
Direct-direct/mes (DD3)	4/2		3

FIGURE 5.27 Distortion factor versus modulation index. (From Neacsu DO, Tutorial Presented at IECON'01: The 27th Annual Conference of the IEEE Industrial Electronics Society 2001, IEEE Paper 0-7803-7108-9/01. With permission.)

By normalization to this waveform, the monotony of the plots changes. Results for the most well-known methods derived from SVM are shown in Figure 5.27.

5.9   OVERMODULATION FOR SVM

It has been shown that the maximum modulation index of the regular SVM algorithm is achieved when the circular trajectory with the largest radius becomes tangential to the external hexagon formed with the switching vectors (see Figure 5.11). The linearity of the PWM ends at this point.

Many applications, however, require more voltage up to the six-step mode. Operation between these two limits is called overmodulation and was presented in Chapter 4. Let us see here how an overmodulation algorithm can be defined under SVM.
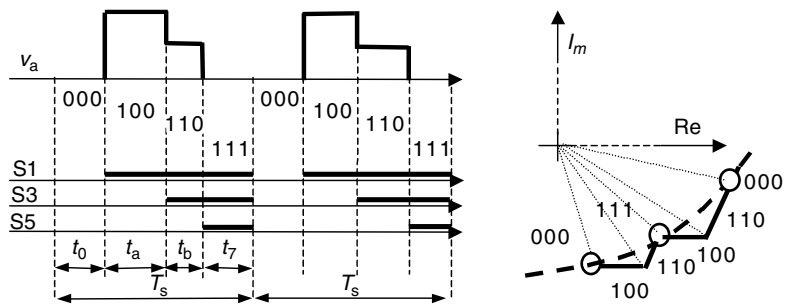

FIGURE 5.28 Pulse generation with method S-D-H.

First, the operation is characterized by a trajectory of the averaged space vector along a circle of radius $m > 0.866$ as long as the circle arc is located within the hexagon and along the hexagon sides in the remaining portions. The same Equations (5.30) are used for PWM generation when the tip of the averaged space vector is on the circular trajectory. For points that lie on the sides of the hexagon, there is no zero state ($t_0 = 0$) and the following equations are used for the active states

$$t_a = T_s \frac{\sqrt{3}\cos\alpha - \sin\alpha}{\sqrt{3}\cos\alpha + \sin\alpha}$$
$$t_b = T_s \frac{2\sin\alpha}{\sqrt{3}\cos\alpha + \sin\alpha} \tag{5.52}$$

At $m = 0.952$, the trajectory shows at the hexagon, and no portions move into the circular locus. In order to advance towards the six-step operation, *Operation Mode II* is defined. This time, the velocity of the tip of the averaged space vector is controlled. The higher the modulation index is expected to be, the higher is the velocity in the center of each hexagon side and the lower in the corners. This mode converges smoothly into a six-step operation when the trajectory is limited to six discrete positions in the complex plane. The structure of a pulse over each sampling interval is composed of only two active states. Zero states are never used.

Both operation modes are characterized by nonlinear transfer characteristics with addition of harmonics that jeopardize the harmonic performance. This is natural because the six-step operation has been already shown to have important harmonics.

5.10   VOLT-PER-HERTZ CONTROL OF PWM INVERTERS

Chapter 4 introduced the *volt-per-hertz* control associated with PWM techniques. It has also been shown that industry uses PWM with different numbers of pulses for different fundamental frequency intervals (Figure 5.30). A larger frequency ratio is therefore considered for low frequencies, whereas the power converter operates at high fundamental frequencies with a smaller frequency ratio. Extension of this method to SVM control is presented next.
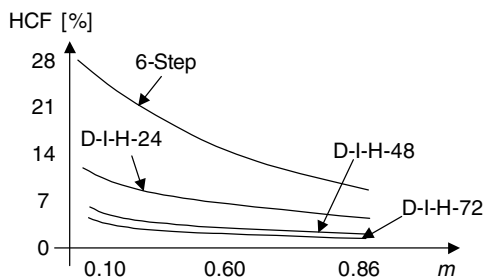

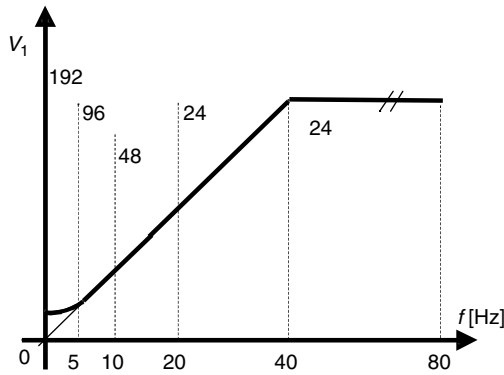**FIGURE 5.29** HCF for different numbers of sampling intervals over the fundamental.

FIGURE 5.30 Volt-per-hertz control.

SVM control of a gate turn-off (GTO) inverter with a switching frequency below 960 Hz is shown in Figure 5.30 [45]. The switching frequency is limited to GTO devices and has wide enough pulses to compensate for the voltage drop across the stator resistance. The following operation modes are accordingly obtained:

- At higher frequencies: An operation mode with a constant voltage is preferred in order not to exceed the induction machine nominal value. The voltage is kept constant between 40 and 80 Hz with an optimal SVM having 24 pulses.
- At lower frequencies: A PWM method is used with $V_1/f =$ constant and a number of pulses on different frequency intervals: 24 pulses, ... 20–40 Hz; 48 pulses, ... 10–20 Hz; 96 pulses, ... 5–10 Hz; 192 pulses, ... <5 Hz.

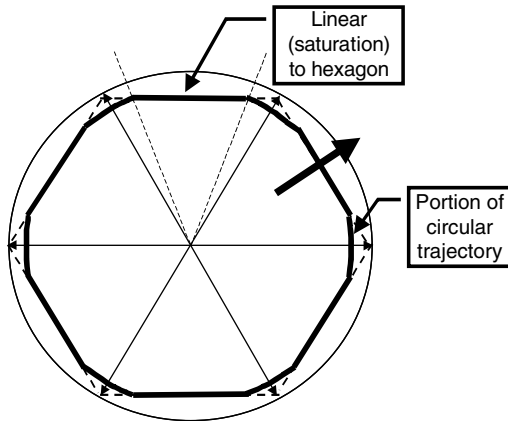The specifics of SVM for each operation mode are pesented in Figure 5.31.

FIGURE 5.31 Operation Mode (I).

5.10.1 LOW-FREQUENCIES OPERATION MODE

The relation $V_1/f = $ constant can be written as $V_1QT = $ constant, where Q is the number of pulses over the fundamental period (also called *frequency ratio*). For each frequency interval shown in Figure 5.30, the magnitude and RMS of the output phase voltage take values within a finite interval and the vectorial representation of this operation brings us inside a circular corona (for example, between V_{s1} and V_{s2} in Figure 5.32).

   The time allocated to the switching vectors neighboring a desired space vector position has been defined previously by Equations (5.30). These equations can be seen as t_a, $t_b = $ constant $^* V_s ^* T_s$ for a given direction on the complex plane. The similarity between these forms of Equations (5.30) and the *volt-per-hertz* control condition ($V_1QT = $ constant) implies a possible modification of the RMS value of the output voltage by adjusting the sampling interval T_s while both t_a, t_b are kept constant (Figure 5.33).

   In order to decrease the frequency, the sampling period is increased by enlarging the zero-states' intervals. When the period doubles, the transition to the next domain occurs. This domain will be characterized by twice the number of pulses achieved by splitting the previous sampling period into two intervals. The use of the same time constants in all low-frequency operation modes is therefore possible, improving microcontroller and memory look-up table use. Figure 5.34 presents all possible positions of the tip of the space vector with the magnitude equaling the condition for transition from one domain to the next. Intermediary magnitude values are easily generated on the basis of the same time constants by enlarging the zero-state intervals. This figure is also important as it shows the positions that need to have time constants stored in memory. All the other positions will use the same time constants (t_a, t_b). Considering all other symmetries of a three-phase system limits the total number of memory locations to

$$N_{\mathrm{ML}} = 2\left[1 + \frac{m}{12}\right] \tag{5.53}$$
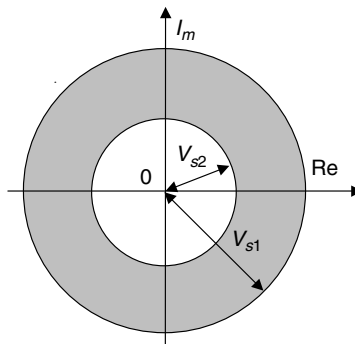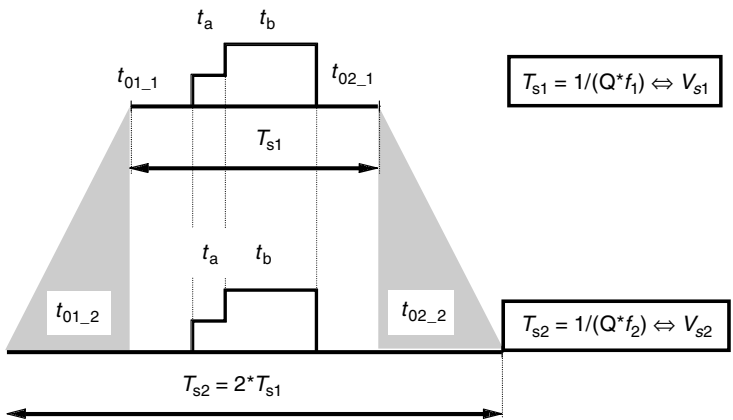

FIGURE 5.32 Circular corona.

FIGURE 5.33 Pulse width changes over a circular corona in the complex plane.

5.10.2 HIGH-FREQUENCY OPERATION MODE

The operation of the induction machine in high fundamental-frequency range implies limitation of the voltage. The same PWM pattern is supposed to be used for all these frequencies. Due to the nature of the high-frequency operation, the number of pulses in this pattern is limited (24 pulses in our example) and the harmonic results are not very good. It is a good practice to define an optimal PWM algorithm on the basis of harmonic elimination or global harmonic minimization for this domain.

Reducing this pattern to a 30° sector when considering the symmetries within a three-phase system shows a position on the real axis — one intermediary position and the last one on the 30° direction. There is a degree of freedom in neglecting Equations (5.30) and in defining a new set of optimal time constants instead of calculating t_a, t_b on the basis of the optimization constraints. For instance, one can set the
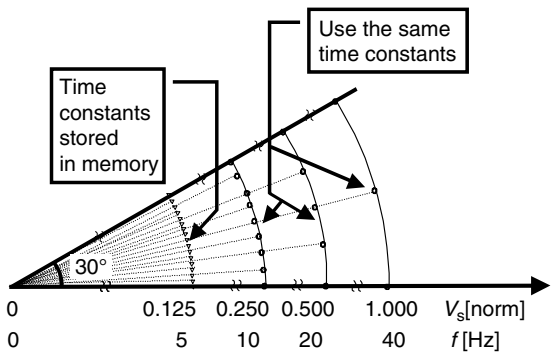

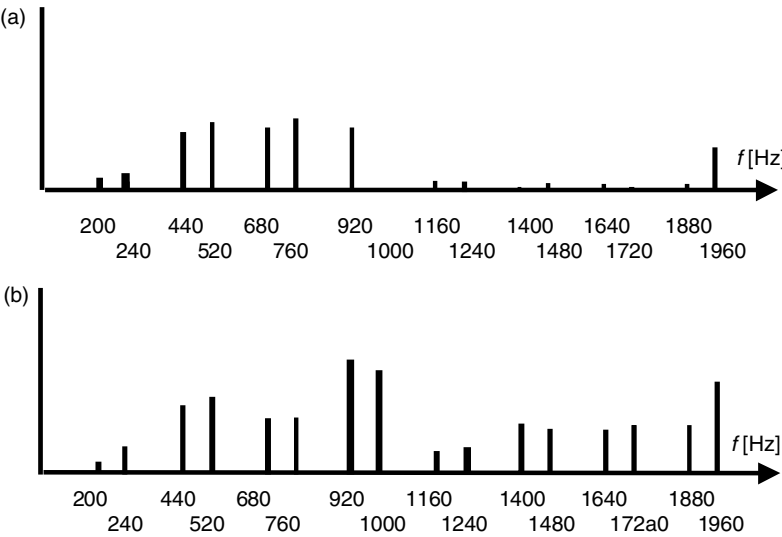**FIGURE 5.34** Operation within a 30° sector.

FIGURE 5.35 Spectra for different PWM patterns at 40 Hz. (a) Optimal PWM at fundamental frequency of 40 Hz (b) Optimal SVM at fundamental frequency of 40 Hz.

fundamental voltage at a desired value and limit both lowest harmonics as $\min(V_5^2 + V_7^2)$. This implies replacing the time constants calculated with Equations (5.30) by

$$
\begin{aligned}
t_a &= 0.793 T_s \\
t_b &= 0.152 T_s
\end{aligned}
\tag{5.54}
$$

These values yield both 5th and 7th harmonics below 3% of the fundamental of the output voltage. These harmonic results are shown in Figure 5.35.
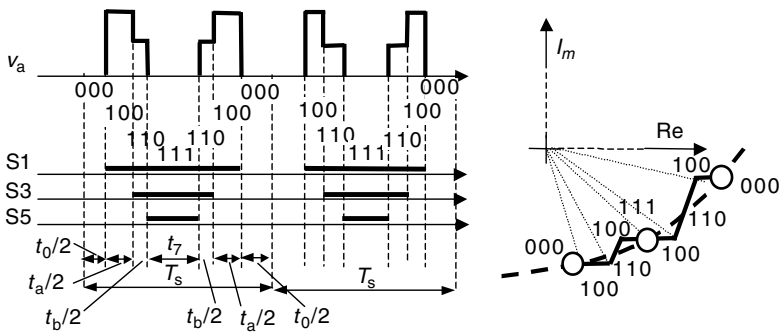

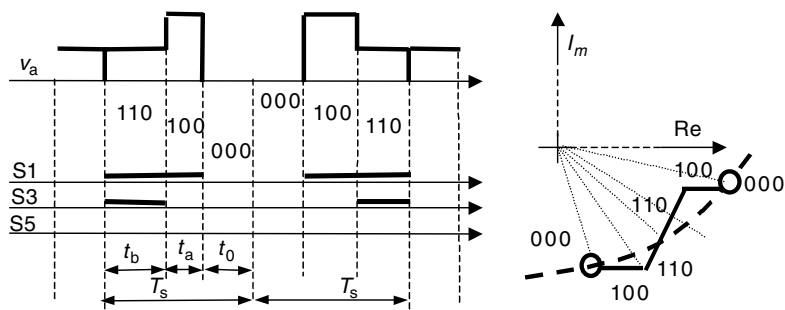**FIGURE 5.36** Pulse generation with method SGS.

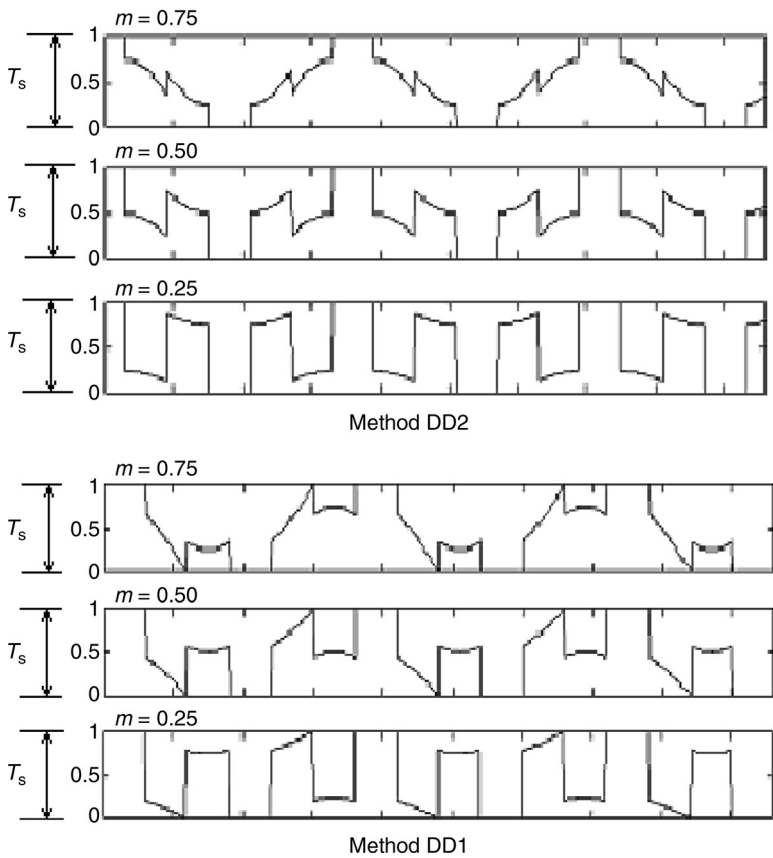**FIGURE 5.37** Modified space vector modulation.

FIGURE 5.38 Pulse generation with methods DD1 and DD2 for different modulation indices.
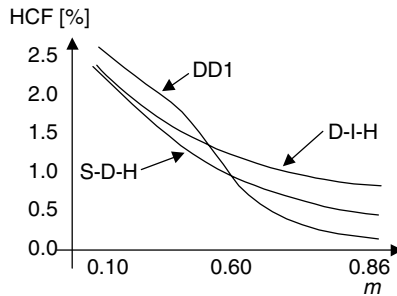
FIGURE 5.39 HCF for several modulation methods calculated for $f_1 = 50$ Hz, $f_{sw} = 3.6$ kHz.

5.11 CONCLUSION

The space vector theory has been known for more than half a century, but only during the last 20 yrs, it has been consistently used in the control of three-phase converters. Details of PWM generation on the basis of vector representation as well as use of this concept in motor drives are the subjects of this chapter. All SVM variations are reviewed and the advantages of discontinuous reference functions are also outlined.

5.12 PROBLEMS

P.5.1 Write relationship for Park/Clarke direct transforms and inverse transforms and prove the meaning of coefficients for power conservation and for magnitude conservation.

P.5.2 Establish the mathematical expressions for waveforms in Figure 5.22. Consider each one as a phase function and write the mathematical expressions for the other two phases taking into account the phase shifts of 120 and 240°.

P.5.3 Consider functions defined in P.4.2. and define a new base in the vector space similar to the base defined in Equation (5.4), Equation (5.5), and Equation (5.6). Then define a vector transform able to convert the $(d, q, 0)$ quasi-DC coordinates into phase voltages as shaped in Figure 2.22. Use a computer program (MathCAD, Matlab) to implement these relationships and run the program to plot control functions.

P.5.4 Imagine a PWM pattern synchronized with the fundamental period and a count of 24 pulses on one period:

- Draw the spatial distribution of the tip of the voltage vector.
- For each discrete position thus determined, calculate the amount of time associated with each neighboring active vectors using Equation (5.29) and

Equations (5.30) for a modulation index of 0.55 defined as in Equation (5.31).

- Consider the active vectors in the middle of the sampling interval and draw the time evolution of the voltage on the first phase during the first sector (method D-I-H), using information from Figure 5.14.

P.5.5 If a three-phase inverter is supplied from a three-phase central-point rectifier with very weak filtering or without filtering, calculate the maximum voltage we can have at the inverter output without overmodulation. Use Figure 5.11 and Equation (5.31) after definition of the minimum value of the rectified voltage (V_{DC}). Consider the grid RMS voltage as 120 V per phase.

P.5.6 Demonstrate Equation (5.41) to Equation (5.46).

P.5.7 Write Equation (5.48) for each sector, using the active switching vectors from Figure 5.14 and their orthonormal coordinates in the complex plane.

P.5.8 Use Figure 5.36 and define the instants for turning ON each of the six IGBT switches.

- Write their expressions as a delay from the beginning of the sampling interval: For instance, $f(S1) = t_0/2$, $f(S2) = T_s - t_0/2$, and so on. Replace definitions from Equation (5.41) to Equation (5.46) for each sector. Organize these results as a flowchart to be implemented in a microcontroller with a center-aligned PWM generator.
- Write a computer program and draw the evolution of the calculated ON-time. Compare the results with Figure 5.15.

P.5.9 Do the same as in P.5.7. with the switching sequence shown in Figure 5.37. Compare results with Figure 5.38.

P.5.10 Explain an algorithm to take advantage of the best HCF from Figure 5.25 and Figure 5.39. at any modulation index. How can we modify the switching reference function to ensure a smooth transition from one method to another?

REFERENCES

1. Park RH, Two-reaction theory of synchronous machines. *AIEE Trans.*, 48: 716–730, 1929. 52: 352–355, 1933.
2. Kron G, The Application of Tensors to the Analysis of Rotating Electrical Machinery, Schenectady, NY, USA, General Electric Review, 1942.
3. Stanley HC, An analysis of the induction motor. *AIEE Trans.*, 57: 751–755, 1938.
4. Kovacs KP and Racz I, Transiente Vorgange in Wechselstrommachinen. Budapest, Hungary, Akad Kiado, 1959.
5. Stepina J, Raumzeiger als Grundlage der Theorie der Elktrischen Maschinen. *etz-A*, 88(23): 584–588, 1967.
6. Serrano-Iribarnegaray L., The modern space-phasor theory, Part I & Part II, *ETEP J.*, 3(2): March/April, 3 May/June 1993.

7. Murai Y and Tsunehiro Y, Improved PWM Method for Induction Motor Drive Inverters, IPEC, Tokyo, 1983, pp. 407–417.
8. Holtz J, Lammert P, and Lotzkat W, High Speed Drive System with Ultrasonic MOSFET-PWM-Inverter and Single-CHIP Microprocessor Control, Conference Record 1986 IEEE Industry Applications Society Annual Meeting, Part 1, Denver Colorado, USA, pp. 12–17.
9. Van der Broeck, Skudelny HC, and Stanke G, Analysis and Realization of a Pulse Width Modulator Based on Voltage Space Vectors, IEEE-IAS Annual Meeting Conference Record, Denver, USA, 1986, pp. 244–251.
10. Fukuda S, Hasegawa H, and Iwaiji Y, PWM technique for inverter with Sinusoidal Output Current, 19th Annual IEEE Power Electronics Specialists Conference, Kyoto, Japan, vol. 1, 1988, 11–14 Apr, pp. 35–41.
11. Granado J, Harley RG, and Diana G, Understanding and designing a space vector pulse-width-modulator to control a three phase inverter, *Trans. SAIEE*, 80: 29–37, 1989.
12. Halmos P, *Finite-Dimensional Vector Spaces*, Springer-Verlag, New York, 1986.
13. Abrahamsen J, Pedersen JK, and Blaabjerg F, State-of-the-art of Optimal Efficiency Control of Low Cost Induction Motor Drives. PEMC'96, vol 2, Budapest, Hungary, 2–4 September 1996, pp. 163–170.
14. Murai Y, Gohshi Y, Matsui K, and Hosono I, High-frequency split zero-vector PWM with harmonic reduction for induction motor drive, *Trans. IA*, 28(1): 105–112, 1992.
15. Murai Y, Sugimoto S, Iwasaki H, and Tsunehiro Y, Analysis of PWM Inverter Fed Inductions Motors for Microprocessors, Proceedings IEEE/IECON, San Francisco, CA, USA, 10–14 November, pp. 58–63, 1983.
16. Fukuda S, Iwaji Y, and Hasegawa H, PWM technique for inverter with sinusoidal output current, *IEEE Trans. PE*, 5: 54–61, 1990.
17. Andersen EC and Hann A, Influence of the PWM control method on the performance of frequency inverter induction machine drives. *ETEP*, 3(2): 151–160, 1993.
18. Holtz J, Pulsewidth modulation — a survey, *IEEE Trans. IE*, 39(5): 410–420, 1992.
19. Holtz J, Pulsewidth modulation for electronic power conversion. *Proc. IEEE*, 82(8): 1194–1212, 1994.
20. Handley PG and Boys JT, Space vector modulation — an engineering review. *PEVSD*, London, UK, 87–91, 1991.
21. Neacsu D, Space Vector Modulation, Seminar IEEE-IECON, San Jose, CA, USA, December 2001.
22. Neacsu D, Stincescu R, Raducanu I, and Donescu V, Fuzzy Logic Control of an PWM V/f Inverter-Fed Drive, ICEM'94, vol 3, Paris, France, 1994, pp. 12–17.
23. Saetieo S and Torrey D, Fuzzy logic control of a space vector PWM current regulator for three-phase power converter, *IEEE Trans. PE*, 13(3): 419–426, 1998.
24. Enjeti P and Shireen A, A new technique to reject DC-link voltage ripple for inverters operating on programmed PWM waveforms, *IEEE Trans. PE*, 7(1): 171–180, 1992.
25. Schermann M., Schroedl M, Methods of generating the voltage space vector by fast real-time PWM, *IEEE-PCC*, Yokohama, Japan, 1993, pp. 322–327.
26. Jacobina CB, Nogueira Lima AM, da Silva ERC, Alves RNC, Seixas PF., Digital scalar pulse-width modulation: a simple approach to introduce non-sinusoidal modulating waveforms, *IEEE Trans. PE*, 16(3): 351–359, May 2001.
27. Lai YS and Bowes SR, A universal Space Vector Modulation Strategy Based on Regular-Sampled Pulse-Width Modulation [Invertors]. Proceedings IEEE IECON 22nd, vol 1, 1996, pp. 120–126.

28. Bowes SR and Lai YS, The relationship between space-vector modulation and regular-sampled PWM, *IEEE Trans. IE*, 44(5): 670–679, 1997.
29. Sun J and Grotstollen H, Optimized Space Vector Modulation and Regular-Sampled PWM: a Reexamination, Conference Record of the 1996 IEEE Thirty-First IAS Annual Meeting IAS '96, San Diego, CA, USA, vol. 2, pp. 956–963, 6–10 October, 1996.
30. Holmes DG, A unified modulation algorithm for voltage and current source inverters based on AC–AC matrix converter theory, *IEEE Trans. IA*, 28(1): 31–40, 1992.
31. Neacsu D and Lucanu M, Output Waveform Optimization of the SVM Inverters, Proceedings of National Conference Electric Drives, Iasi, Romania, 22–24, October 1992, pp. B1–B6.
32. Holmes DG, The Significance of Zero Space Vector Placement for Carrier Based PWM Schemes, Conference Record of the Thirtieth IAS Annual Meeting IEEE Industry Applications Conference, IAS '95, Orlando, FL, USA, vol. 3, pp. 2451–2458, 8–12 October, 1995.
33. Kolar JW, Ertl H, and Zach FC, Calculation of the Passive and Active Component Stress of Three-Phase PWM Converter, Proceedings EPE, Aachen, Germany, 1989, pp. 1303–1311.
34. Alexander DR and Williams SM, An Optimal PWM Algorithm Implementation in a High Performance 125 kVA Inverter, Conference Proceedings of the 1993 Eighth Annual Applied Power Electronics Conference and Exposition, APEC '93, San Diego, CA, USA, pp. 771–777, 7–11 March, 1993.
35. van der Broeck H, Analysis of the Harmonics in Voltage-Fed Inverter Drives Caused by PWM Schemes with Discontinuous Switching Operation, Proceedings EPE'91, pp. 3/261–3/266.
36. Houldsworth JA and Grant DA, The Use of Harmonic Distortion to Increase the Output Voltage of a Three-Phase PWM Inverter, *IEEE Trans. IA*, IA-20: 1224–1228, 1984.
37. Hava AM, Kerkman RJ, and Lipo TA, A High Performance Generalized Discontinuous PWM Algorithms, IEEE Transactions on Industry, Applications, vol. 34, no. 5, pp. 1059–1071, September–October, 1998.
38. Trzynadlowski AM and Legowski S, Minimum-Loss Vector PWM Strategy for Three-Phase Inverters, *IEEE Trans. PE*, 9(1): 26–34, 1994.
39. Chung DW and Sul SL, Minimum-Loss PWM Strategy for a 3-Phase PWM Rectifier. Proceedings of the 28th Power Electronics Specialists Conference PESC, St. Louis, MO, USA, vol. 2, pp. 1020–1026, 22–27 June, 1997.
40. Lai RS and Ngo KDT, A PWM Method for Reduction of Switching Loss in a Full-Bridge Inverter, *IEEE Trans. PE*, 10(3): 326–332, 1995.
41. Trzynadlowski AM, Kirlin RL, and Legowski S, Space Vector PWM Technique with Minimum Switching Losses and a Variable Pulse Rate, *IEEE Trans. IE*, 44(2): 173–181, 1997.
42. Faldella E and Rossi C, High efficiency PWM Techniques for Digital Control of DC/AC Converters. Conference Proceedings of the Ninth Annual Applied Power Electronics Conference and Exposition, APEC '94, Orlando, FL, vol. 1, pp. 115–121, February 13–17, 1994.
43. Perruchoud PJP and Pinewski PJ, Power losses for Space Vector Modulation Techniques, IEEE-WPET, Dearborn, MI, USA, 1996, pp. 167–173.
44. Ahmad RH, Karady GG, Blake TD, and Pinewski P, Comparison in Space Vector Modulation Techniques Based on Performance Indexes and Hardware Implementation, 23rd International Conference on Industrial Electronics, Control and

Instrumentation, IECON 97, New Orleans, LA, USA, vol. 2, pp. 682–687, 9–14 November, 1997.

45. Lucanu M and Neacsu D, Optimal *V/f* Control for Space Vector PWM Three-Phase Inverters, *Eur. Trans. EPE*, 5(2): 115–120, 1995.

46. Prasad VH, Borojevic D, and Dubovsky S, Comparison of High-Frequency PWM Algorithms for Voltage Source Inverters, Conference Proceedings of the 13th Annual Applied Power Electronics Conference and Exposition, APEC 1997, Atlanta, GA, USA, pp. 857–863, 23–27 February, 1997.